Ordered Self-Assembled Monolayers of Peptide Nucleic Acids with DNA Recognition Capability

C. Briones,[1] E. Mateo-Marti,[1] C. Gómez-Navarro,[2] V. Parro,[1] E. Román,[2] and J. A. Martín-Gago[1,2,*]

[1]*Centro de Astrobiología (CSIC-INTA), C. Ajalvir, Km. 4, 28850 Torrejón de Ardoz, Madrid*

[2]*Instituto de Ciencia de Materiales de Madrid (CSIC), Cantoblanco, 28049 Madrid, Spain*

(Received 19 April 2004; published 11 November 2004)

We report on the formation of ordered self-assembled monolayers (SAMs) of single-stranded peptide nucleic acids (ssPNA). In spite of their remarkable length (7 nm) thiolated PNAs assemble standing up on gold surfaces similarly to the SAMs of short alkanethiols. SAMs of ssPNA recognize complementary nucleic acids, acting as specific biosensors that discriminate even a point mutation in target ssDNA. These results are obtained by surface characterization techniques that avoid labeling of the target molecule: x-ray photoemission, x-ray absorption and atomic force microscopy.

DOI: 10.1103/PhysRevLett.93.208103 PACS numbers: 87.15.By, 68.37.Hk, 68.47.Pe, 79.60.–i

Self-assembly and self-organization are the main strategies used in nature to permit life to emerge from its building blocks, and have inspired new trends in nanotechnology based on a bottom-up approach [1]. In particular, a lot of effort has been devoted to the understanding of the main mechanisms that drive the spontaneous self-organization of molecular films on surfaces [2]. Alkanethiol layers have been extensively studied due to their relevant technological properties and their outstanding capability to form self-assembled monolayers (SAMs) [3]. Based on such knowledge, thiolated DNA has also been immobilized on gold surfaces [4]. Nevertheless, DNA usually forms disordered formless globular structures, or requires the coimmobilization of spacer thiols leading to mixed monolayers. Poorly ordered DNA layers show a reduced bioactivity, mainly because of the strong electrostatic molecule-molecule and molecule-surface interactions [4–6]. Therefore, uncharged nucleic acid analogues could be suitable candidates to grow bioactive SAMs with efficient DNA recognition capability. Peptide nucleic acid (PNA) is an achiral and uncharged DNA mimic where the sugar-phosphate backbone has been replaced with a peptidelike *N*-(2-aminoethyl)glycine polyamide structure, to which the nucleobases are connected by methylenecarbonyl linkages [7,8]. PNA is characterized by its capability to strongly and specifically bind to complementary DNA according to the Watson-Crick rules for base pairing [9]. These unique properties make PNA a suitable candidate for biosensor applications. In this Letter, we report on the formation of ordered SAMs of single-stranded PNA (ssPNA) molecules on gold surfaces, adsorbed from water, stable in air and with efficient and specific ssDNA recognition capability. Such structural and functional characterization has been performed through label-free techniques such as x-ray photoemission spectroscopy (XPS), x-ray absorption near-edge spectroscopy (XANES) and atomic force microscopy (AFM).

We have analyzed the structure of immobilized layers of two different cysteine-modified ssPNA oligomers: P-G142 (Cys-O-O-AATCCCCGCAT), and P-M41 (Cys-O-O-GCCATCTCT) (amino to the carboxyl terminus). These sequences were chosen for their relevance in virology and medicine: P-G142 corresponds to the capsid protein VP1 of foot-and-mouth disease virus (FMDV) [10] and P-M41 to the reverse transcriptase gene of human immunodeficiency virus (HIV) [11]. The cysteine moiety at their amino terminus provides the thiol group that allows immobilization on gold surfaces. The "O" spacer unit is a 1.5 nm long molecule of 8-amino-3,6-dioxaoctanoic acid. The total length of the ssPNAs can be estimated to be 7.1 nm (P-G142) and 6.4 nm (P-M41), considering a helical rise of 4.2 nm with 13 base pairs per turn [12,13]. Target ssDNA molecules were designed in antisense orientation with respect to PNAs. They are 31 nucleotides long, correspond to the sequences of wild type and mutant FMDV or HIV [10,11], and are complementary to P-G142 or P-M41 at their 11 or 9 central bases, respectively. We used perfect matching and single nucleotide mismatching ssDNA targets (the later bearing mutations $G \rightarrow A$ or $A \rightarrow T$ at their central positions).

Immobilization experiments of ssPNA were performed in a humid chamber at 22 °C for 4 h, on Au(111). After immobilization, the crystals were vigorously rinsed in H_2O to avoid unspecific adsorption. PNA-DNA hybridization was carried out at low ionic strength, in a buffer containing 7 mM NaCl and 0.7 mM Na-citrate, *p*H 7.2. The concentration of ssPNA probe varied from 0.1 to 100 μM in different experiments, while that of the ssDNA target was fixed at an optimized value of 100 μM. Hybridization time was 1 h, and temperatures ranged from 41 °C to 58 °C. High-resolution XPS experiments were performed in the Super-ESCA beamline (ELETTRA, Trieste, Italy). The overall resolution of the spectra was around 80 meV. We checked that the samples were not damaged by x-ray radiation.

First, we studied the structure of the ssPNA adlayers by two complementary techniques: AFM and XANES. Figures 1(a) and 1(b) show AFM images of different samples obtained after immobilization of a 1 μM ssPNA solution. A strikingly ordered arrangement of the molecules was observed, with reproducible aligned and meandering patterns. The ordered protrusions are 6 to 7 nm high from the bare surface and their width is 10 to 30 nm. The tip radius of the AFM is smaller than 20 nm, thus the protrusions can be interpreted as groups of molecules standing-up on the surface. A typical line profile of these ordered protrusions is shown in Fig. 1(c). The chemical structure and theoretical length of P-G142 is depicted in Fig. 1(d). The lower apparent height measured by AFM could be related (apart from some degree of flexibility allowed by the PNA backbone) either to a small tilt of the molecule, or to a deformation of the molecular layer induced by the AFM tip. Indeed, both effects were previously observed and tilts in SAMs of alkanethiols up of 30° have been reported [2,3]. Tilted

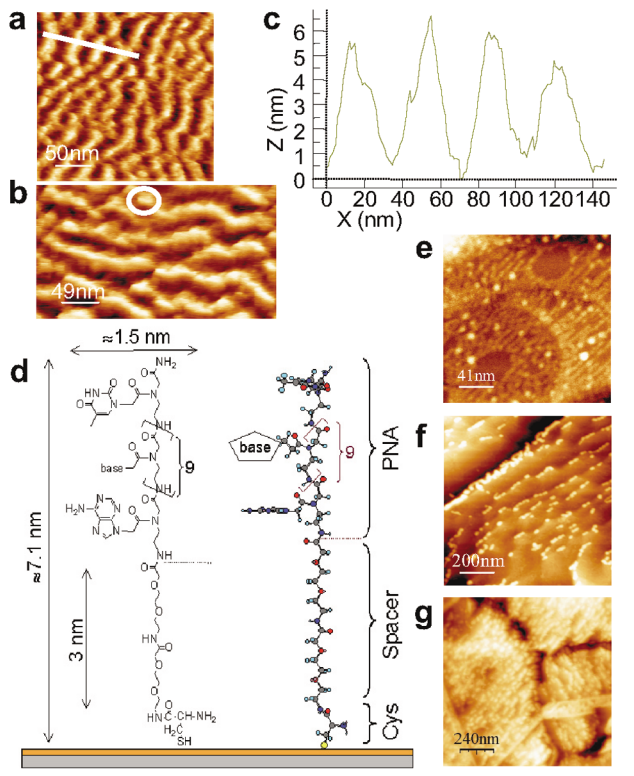

FIG. 1 (color). (a),(b) AFM images recorded in air of P-G142 immobilized at 1 μM on gold surfaces. One individual group of molecules has been encircled in (b). (c) A cross-section profile recorded across the line in (a). (d) Chemical structure and proposed immobilization geometry of P-G142; only the first and last nucleobases are shown. (e) AFM image of P-M41 immobilized at 0.1 μM. The height of the ordered linear features is 1 nm. (f),(g) AFM images for 0.5 μM concentration of P-G142 showing that the upper part of the steps act as nucleation sites for adsorption of the ssPNA layer.

ssPNA chains could facilitate noncomplementary hydrogen bonding between nucleobases placed at different chain positions, stabilizing the lateral contacts among molecules that lead to the ordered arrangement. Moreover, the real height of a molecular layer adsorbed on a surface by tapping mode AFM is an open issue, and deformations up to 50% of the nominal value are frequently reported for soft material [5,6,14]. The meandering structure of the ssPNA layers can be due to the free adsorption of molecules on the surface, with a rotational symmetry around the molecular backbone allowing them to find their closest neighbor for intermolecular contacts.

We performed a systematic study to quantify the dependence of the ordering with the concentration of the immobilized ssPNA probe. Some representative results are shown in Fig. 1. Figure 1(e), obtained with 0.1 μM ssPNA, shows linear features composed by segments of up to 10 nm (AFM resolution) running parallel to the surface crystallographic directions of the crystal. Two bare areas are imaged, from which the apparent height of the features was measured to be smaller than 1 nm, a value similar to that previously described for ssDNA by AFM imaging [15]. These features can be interpreted as individual molecules lying on the gold surface, anchored by their thiol motif and possibly the carbonyl or amino groups of some chemisorbed nucleobases. Different sets of experiments showed that the transition from individual lying molecules to standing-up groups of them is favored by increasing the concentration. Figure 1(f) was recorded with 0.5 μM ssPNA: the layer is not complete and groups of molecules standing-up form aligned islands anchored to the upper part of the step edges. We checked that these islands correspond to a molecular layer of soft material by recording force-distance curves. Figure 1(g) shows a large area where aligned features follow crystallographic directions in three adjacent gold terraces. These images suggest a nucleation mechanism for the growth of islands from the step edges. This is also the reason for the alignment along the main crystallographic surface directions. Therefore, we propose a mechanism in which the formation of a bioSAM of ssPNA goes through two steps: i) ssPNAs condensate on the surface and are adsorbed as lying molecules; ii) at a certain coverage density the layer undergoes a phase transition and the molecule backbone realigns perpendicular to the surface. A similar mechanism was described for SAMs of alkanethiols [16] and it demonstrates the importance of the intermolecular interaction in self-assembly. Interestingly, increasing the coverage makes SAMs of ssPNA to rearrange into a stand-up conformation without requiring the addition of alkanethiols or other adjuvant molecules that would lead to mixed monolayers, as reported for ssDNA [4,14] and ssPNA [17]. AFM images in water showed very similar morphologies to those shown in Fig. 1, although lying molecules were not detected. Therefore, the H bonds

between ssPNA and water molecules could favor the standing-up geometry even for individual molecules at low coverage.

This structural model derived from the AFM images is quite surprising because of the extraordinary length of the immobilized PNA molecule that generates the bioSAM with respect to alkanethiol SAMs, which typically range from 0.2 to 2.5 nm high [3]. In order to support the preferential orientation of the molecules derived from AFM, we used a complementary structural technique as XANES. The evolution of the XANES spectra for the SAMs of ssPNA at 1 μM was recorded at the N threshold for different incident angles [Fig. 2(a)]. The spectra can be decomposed in two sharp π^* and a broad σ^* peak transitions. The energy shift between π^* and σ^* features is in agreement with previously published XANES spectra of DNA on gold surfaces [18]. The polarization of the synchrotron radiation with respect to the molecular orbital contributing to the signal could mask or enhance a particular transition. Molecules adsorbed randomly, without any preferential orientation, produce overlapping spectra at different incident angles. On the contrary, ordered molecules show clear differences between spectra recorded at different emission angles, which mainly influence the π^*/σ^* ratio. This methodology has been used for finding a preferential orientation of liquid crystal alignment [19] and for dried glycine [20]. In our case the π^* transition is enhanced as the light polarization vector approaches normal emission [Fig. 2(a)]. Since most of the π^* orbitals lie along the backbone of the PNA and the σ^* are parallel to the nucleobases plane, the data indicate that the axes of the PNA stand perpendicular to the surface, in agreement with the arrangement observed by AFM [Figs. 1(a) and 1(b)]. Therefore, both techniques support a structural model in which ssPNA molecules self-assemble on gold surfaces similarly to alkanethiol molecules. Two main

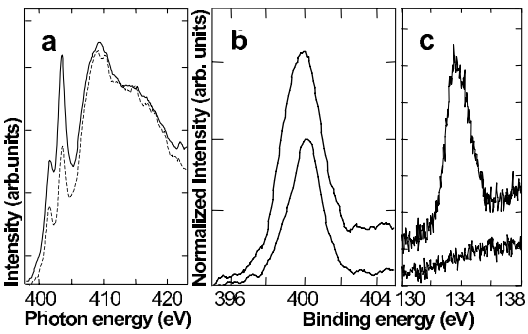

FIG. 2. XANES spectra, normalized to the σ^* intensity, at the N1s edge recorded at different angles between the surface normal and the x-ray polarization vector: 90° (dotted line) and 20° (solid line). (b),(c) XPS spectra, normalized to the Au4f, of the N1s core level peak (b) and P2p peak (c) before (lower curve) and after (upper curve) hybridization of the bioSAM of 1 μM P-G142 with the complementary ssDNA.

reasons can account for the clear advantage of ssPNA over ssDNA in the formation of SAMs: i) the lack of charged groups in the PNA backbone avoids electrostatic repulsions either among neighboring molecules or among the solvent counterions [7,9]; ii) although relatively flexible, the PNA molecule is more rigid than DNA due to the planar amide groups of its polyamide backbone [7], and the restricted conformational flexibility of ssPNA has been recently confirmed by single-wavelength anomalous diffraction experiments [21].

To investigate the biological activity of the SAMs of ssPNA and their interaction with complementary ssDNA, a systematic set of XPS experiments was performed. A high-resolution XPS spectrum for N1s recorded at 500 eV of photon energy from an immobilized ssPNA SAM is presented in Fig. 2(b). The maximum of the N1s peak appears at 400.0 eV of binding energy. N1s binding energy for a peptidic backbone has been reported to be around 400.5 eV [22], that of the nucleobase thymine is around 400.9 eV [23], and a small energy shift could be expected for N atoms in different nucleobases. The overall line shape of this peak is analogous to that recently published for DNA [23], with a small component at the left side of the spectrum that could be related to PNA-substrate bonds induced by the fraction of molecules lying on the surface. Figure 2(b) also shows the corresponding spectra after hybridization of complementary ssDNA. We quantified an average increase of the normalized N1s peak ranging from 2.6 to 3.2 times after hybridization. The number of N atoms per ssPNA molecule is 64, and that of the complementary DNA is 116. Therefore, an enhancement of the N signal in a factor of 2.8 could be expected from an approximate atom-counting model. The good agreement between the expected and obtained value suggests that in the optimal conditions the fraction of ssPNA hybridized with DNA target is near 100%. This value is higher than that reported for DNA-DNA hybridization measured with the same technique [6,23]. Furthermore, the hybridization of the target ssDNA produces the emergence of a net P2p peak related to the phosphate groups in the DNA backbone [Fig. 2(c)]. That P signal, together with a two to threefold increase in the N peak, is a clear fingerprint of the hybridization of complementary ssDNA to bioSAMs of ssPNA.

The combined use of XPS and AFM allowed us to construct a model for the mechanism of a PNA-based biosensor. Figure 3(a) represents the N1s/Au4f photoemission signal for different concentrations of the immobilized ssPNA, before and after hybridization with complementary ssDNA. The signal after immobilization is proportional to the concentration of ssPNA on the surface, up to a saturation value at 10 μM that corresponds to the complete blocking of the available absorption sites. For concentrations ranging from 0.1 to 1 μM, the enhancement of the N1s/Au4f signal after hybridiza-

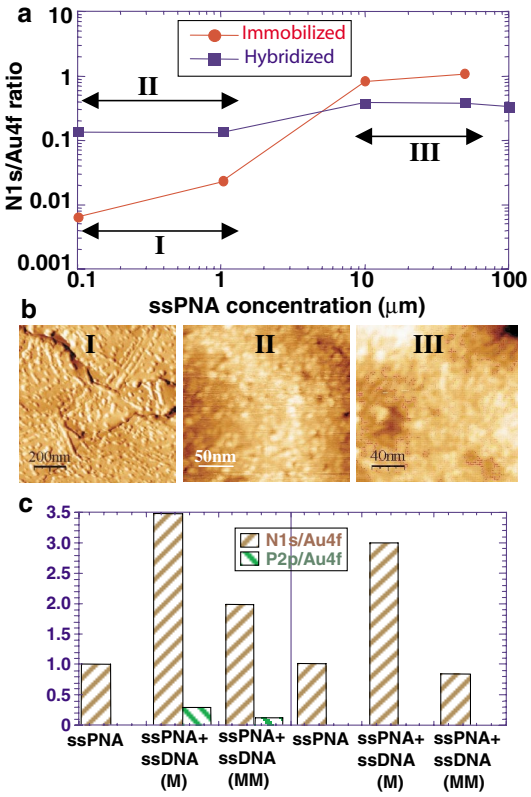

FIG. 3 (color). (a) XPS N1s/Au4f ratio for different concentrations of immobilized P-G142 before and after hybridization with the complementary ssDNA at 100 μM. (b) Typical AFM images recorded in air of different regions of (a). (c) N1s/Au4f and P2p/Au4f ratios before and after hybridization of ssPNA immobilized at 1 μM with the perfectly matched (M) and single mutation mismatched (MM) ssDNA; columns 1–3: P-G142, with hybridization buffer (HB) composed of 7 mM NaCl + 0.7 mM Na-citrate, *p*H 7.2, and washing buffer (WB) composed of 45 mM NaCl + 4.5 mM Na-citrate, *p*H 7.0; columns 4–6: P-M41, and 60 mM NaCl + 6 mM Na-citrate + 0.72% N-lauroylsarcosine as HB and WB.

tion is close to a factor of 3, behaving as a sensitive biosensor. For those higher than 5 μM, the surface is completely covered by ssPNA and the photoemission signal does not change after hybridization, indicating that the bioSAM is not behaving as an active biosensor. Moreover, at those saturating concentrations, the N1s/Au4f ratio after hybridization is lower than in the immobilized case because during the hybridization and washing some of the partially immobilized ssPNA is removed from the surface. Therefore, the bioSAMs of ssPNA present optimal biosensor capacity when immobilized at concentrations of up to 1 μM. The hybridized surface and that immobilized at saturating concentrations show closed and compacted morphologies [Fig. 3(b)]. We have also tested the capability of the bioSAM of ssPNA to discriminate ssDNA targets bearing single point mutations. Post-hybridization washing protocols based on the increase of ionic strength did not allow a complete removal of the mismatched target, while optimized washing buffers including detergents or denaturant agents permitted a perfect match/mismatch discrimination [Fig. 3(c)]. This improved specificity is equivalent to that recently obtained with conventional microarray technologies [24]. Thus, bioSAMs of ssPNA offer the possibility of being employed for mutation screening and single nucleotide polymorphism mapping, relevant features for biomedical and biotechnological applications. Therefore, the unique properties of ssPNA for self-assembly on surfaces could encourage the use of PNA-based biosensors and surface characterization techniques for the detection of label-free nucleic acid targets in biological samples.

This work was supported by the EU, INTA, MCYT (including Grant No. MAT2002-395), and CAM. We are grateful to Super-ESCA staff for technical support, and to S. C. Manrubia, J. Pérez-Mercader, and D. Hochberg for helpful comments on the manuscript.

*Corresponding author.
Electronic address: gago@icmm.csic.es

[1] A. Ulman, *An Introduction to Ultrathin Organic Films, from Langmuir-Blodgett to Self-Assembly* (Academic Press, San Diego, 1991).
[2] J. M. Lehn, Science, **295**, 2400 (2002).
[3] F. Schreiber, Prog. Surf. Sci. **65**, 151 (2000).
[4] T. M. Herne, and M. J. Tarlov, J. Am. Chem. Soc. **119**, 8916 (1997).
[5] H. Wang *et al.*, Surf. Sci. **480**, L389 (2001).
[6] E. Casero *et al.* Langmuir **19**, 6230 (2003).
[7] P. E. Nielsen *et al.*, Science **254**, 1497 (1991).
[8] M. Egholm *et al.*, J. Am. Chem. Soc. **114**, 1895 (1992).
[9] M. Egholm *et al.*, Nature (London) **365**, 566 (1993).
[10] M. A. Martínez *et al.*, Proc. Natl. Acad. Sci. U.S.A. **94**, 6798 (1997).
[11] P. G. Yeni *et al.*, JAMA, J. Am. Med. Assoc. **288**, 222 (2002).
[12] P. Wittung *et al.*, Nature **368**, 561 (1994).
[13] M. Eriksson and P. E. Nielsen, Nat. Struct. Biol. **3**, 410 (1996).
[14] M. Culha *et al.* Anal. Chem.**75**, 6196 (2003).
[15] Y. Lyubchenko *et al.*, Proc. Natl. Acad. Sci. U.S.A. **90**, 2137 (1993).
[16] G. E. Poirier and E. D. Pylant, Science **272**, 1145 (1996).
[17] D. Ozkan *et al.*, Electrochem. Comm. **4**, 796 (2002).
[18] J. N. Crain *et al.*, J. Appl. Phys. **90**, 3291 (2001).
[19] J. Stohr *et al.*, Science **292**, 2299 (2001).
[20] M. L. Gordon *et al.*, J. Phys. Chem. A **107**, 6144 (2003).
[21] V. Menchise *et al.*, Proc. Natl. Acad. Sci. U.S.A. **100**, 12021 (2003).
[22] M. Vinnichenko *et al.*, Appl. Surf. Sci. **201**, 41 (2002).
[23] D. Y. Petrovykh *et al.*, J. Am. Chem. Soc. **125**, 5219 (2003).
[24] O. Brandt *et al.*, Nucleic Acids Res. **31**, e119 (2003).